Electronic Supplementary Information

Two-Dimensional GeAs with Visible Range Band Gap

Chan Su Jung,[‡a] Doyeon Kim,[‡a] Seunghwan Cha,[‡b] Yoon Myung,[c] Fazel Shojaei,[d] Hafiz Ghulam Abbas,[e] Jung Ah Lee,[a] Eun Hee Cha,[b] Jeunghee Park,*[a] and Hong Seok Kang*[f]

[a] Department of Chemistry, Korea University, Sejong 339-700, Korea; [b] Graduate School of Green Energy Engineering, Hoseo University, Asan 336-795, Korea; [c] Department of Nanotechnology and Advanced Engineering, Sejong University, Seoul 05006, Korea; [d] Department of Bioactive Material Science, Jeonbuk National University, Chonju, Chonbuk 560-756, Korea; [e] Department of Nanoscience and Nanotechnology, Jeonbuk National University, Chonju, Chonbuk 560-756, Korea; [f] Department of Nano and Advanced Materials, College of Engineering, Jeonju University, Chonju, Chonbuk 560-759, Korea

Contents

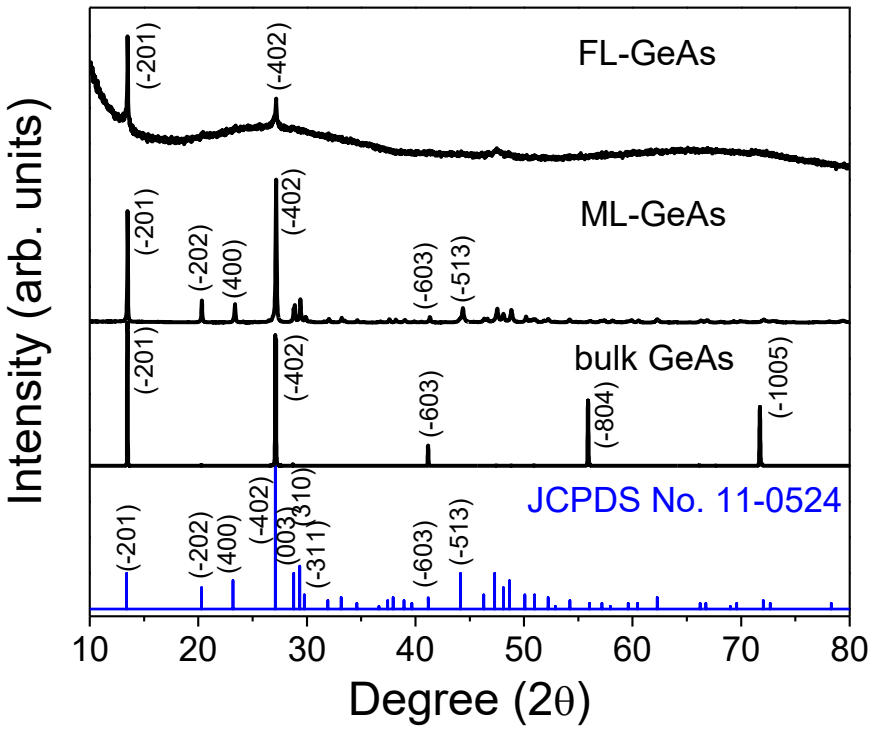

Figure S1. XRD patterns of bulk GeAs, ML-GeAs, and FL-GeAs nanosheets. In the case of FL-GeAs, the NMP suspension was filtered on the AAO membrane. The displayed reference peaks are for monoclinic phase GeAs (JCPDS No. 11-0524, *C*2/*m*, *a* = 15.59 Å, *b* = 3.792 Å, *c* = 9.49 Å, β = 101.28°). The sample peaks well matched those of the reference. The bulk crystal shows only peaks originating from the layer stacking axis. The FL-GeAs nanosheets also show the strong (-201) and (-402) peaks originating from the layer axis.

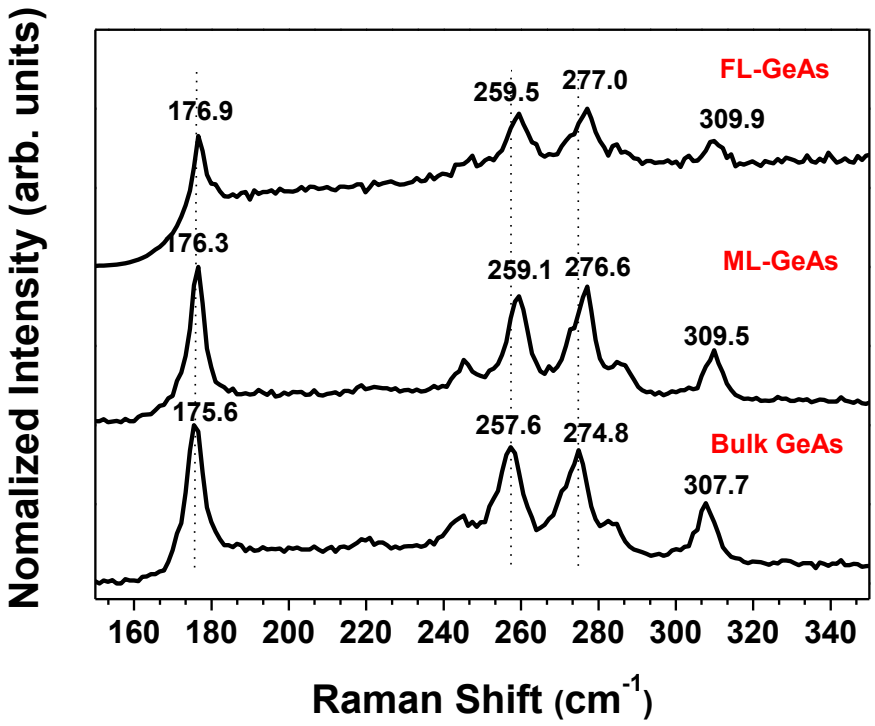

Figure S2. Raman spectra of bulk GeAs, ML-GeAs, and FL-GeAs nanosheets. Excitation at the wavelength of 514 nm was provided from Ar-ion laser. The peaks are similar to those reported by Barreteau *et al* and Yang *et al*.[S1,S2]

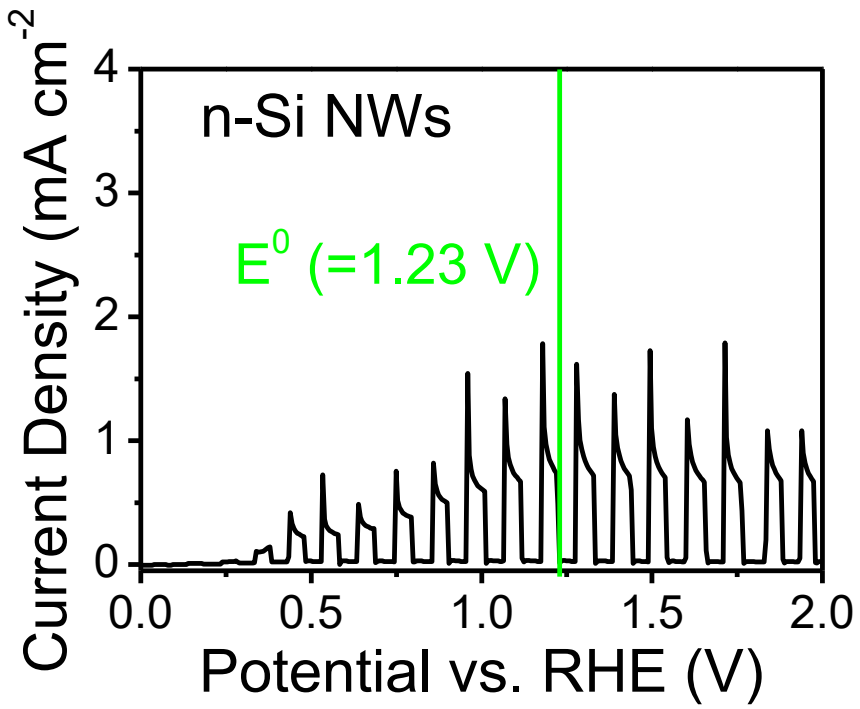

Figure S3. Current density vs. potential (vs. RHE) for *n*-Si photoanodes measured in a 0.1 M Na_2SO_4/0.25 M NaOH (pH 13) electrolyte under AM1.5G (100 mW cm^{-2}) condition.

The bare Si NWs exhibited a photocurrent density of 1.5 mA cm^{-2} at the water oxidation potential E^0 (vertical line, 1.23 V), corresponding to the short-circuit current, J_{SC}. The onset potential or open-circuit voltage (V_{OC}) was estimated to be about 0.35 V, which is higher than that of *p*-GeAs/*n*-Si NWs. We observed significant photocurrent decrease during the first scan owing to the fast oxidation.

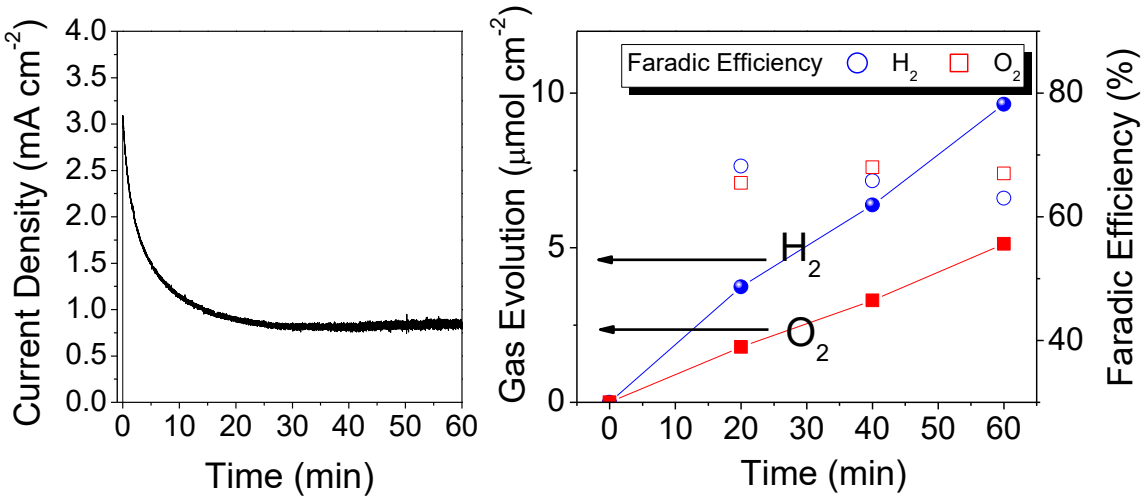

Figure S4. (a) Stability of photocurrent and (b) H_2 and O_2 evolution under the applied potential of 0.9 V vs. RHE.

The initial photocurrent decreased initially (10 min), but becomes steady over 50 min. The 2:1 stoichiometric ratio of H_2:O_2 confirmed the photocatalytic water-splitting reaction: $2H_2O$ (l) $\rightarrow O_2$ (g) + $4H^+$ + $4e^-$ at the anode, and $2H^+ + 2e^- \rightarrow H_2$ (g) at the cathode. Faradic efficiency (*FE*) for the production of H_2 and O_2 was calculated by $FE_{H_2} = \frac{2 \times N_{H_2} \times 96485}{Q}$ and $FE_{O_2} = \frac{4 \times N_{O_2} \times 96485}{Q}$, where N_{H_2} and N_{O_2} are the amounts (mol) of H_2 and O_2, respectively, and Q is the total amount of generated charge in coulomb (photocurrent × time). The obtained Faradic efficiency was about 70%.

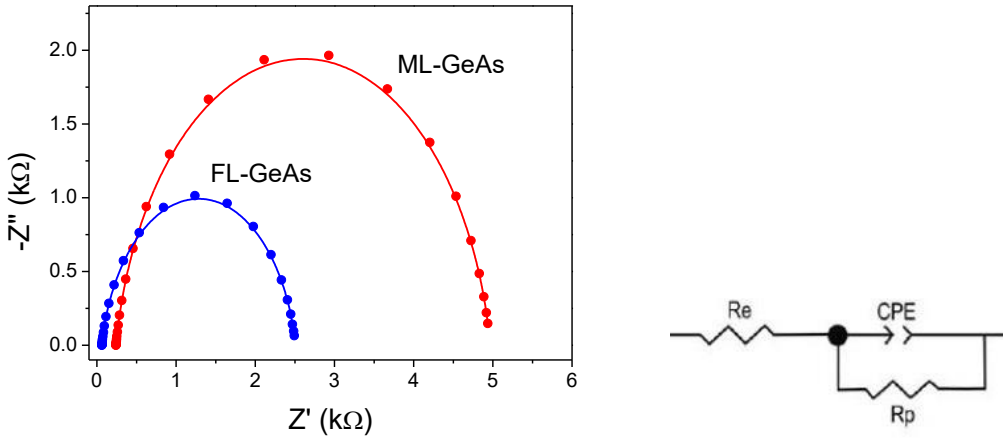

Figure S5. Nyquist plots of ML-GeAs and FL-GeAs nanosheets for EIS experiments in the range from 100 kHz to 0.1 Hz, at a representative potential of 1.23 V (vs. RHE) in a 0.1 M Na_2SO_4/0.25 M NaOH electrolyte. The equivalent circuit is shown on the right.

Electrochemical impedance spectroscopy (EIS) measurements were carried out using a frequency range of 10^5 to 0.1 Hz and an amplitude of 10 mV. The charge-transfer resistance between the electrode and electrolyte, R_{ct}, is a key parameter for characterizing the semiconductor–electrolyte charge transfer process. A semicircle in the Nyquist plot at high frequencies represents the charge transfer process, and R_{ct} is reflected by the diameter of the semicircle. The *x*- and *y*-axes are the real part (Z′) and negative imaginary part (–Z′′) of the impedance, respectively. The simulation of EIS spectra using an equivalent circuit model yielded the R_{ct} values. The fitting parameter R_e represents the internal resistance of the electrolyte, and CPE represents the constant-phase element. From Table S1, the exfoliation decreased R_{ct} by 50% (4.7 and 2.4 kΩ for the ML- and FL-GeAs nanosheets, respectively).

Table S1. Impedance parameters for the equivalent circuit shown in Figure S5.

Sample	R_e (Ω)	R_{ct} (kΩ)	CPE× 10^{-5} (F)
ML-GeAs	242	4.7	1.0
FL-GeAs	63.7	2.4	1.7

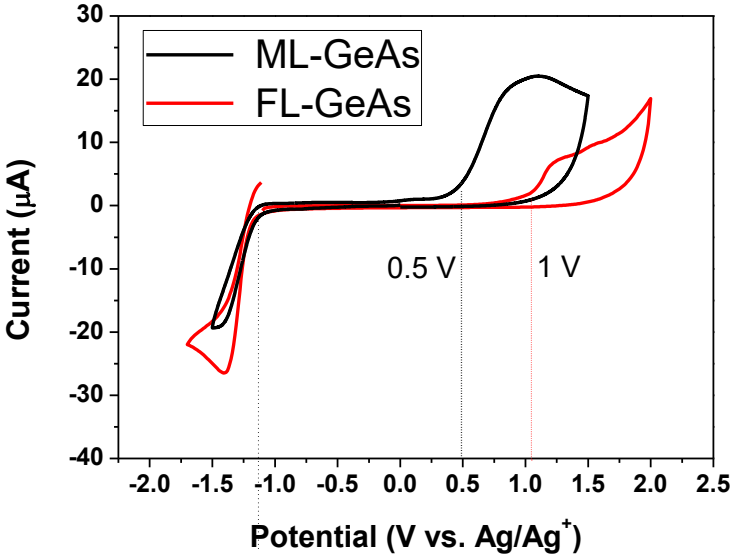

Figure S6. Cyclic voltammetry (CV) data of ML-GeAs and FL-GeAs in 0.25 M tetrabutylammonium hexafluorophosphate ($TBAPF_6$)/acetonitrile electrolyte.

The CV data were measured using a GC electrode as the working electrode, a Pt-wire counter electrode, and a Ag/Ag^+ reference electrode (Ag/0.01 M $AgNO_3$ in 0.1 M $TBAPF_6$/acetonitrile electrolyte). The CV data recorded at a scan rate of 20 mVs^{-1} show strong oxidation peak (E_{Ox}) and reduction peak (E_{Red}). In order to estimate the valence band (VB) and conduction band (CB) positions of the materials, the energy level is calibrated using 1 mM ferrocene/0.25 M $TBAPF_6$/acetonitrile electrolyte. The oxidation/reduction reaction of ferrocene/ferrocenium (Fc/Fc^+) is known to be -4.8 eV below the vacuum level.[S3] We measured the formal potential of Fc/Fc^+ as 0.085 V against a Ag/Ag^+ reference electrode. The VB (E_V) and CB (E_C) energies of the materials were calculated from the oxidation (E_{Ox}) and reduction (E_{Red}) potentials: E_V = -(E_{Ox}+4.715) eV; E_C = -(E_{Red}+4.715) eV, where the onset potential values are relative to the Ag/Ag^+ reference electrode. For ML-GeAs nanosheets, the onset value of E_{Ox} peak is 0.5 V, and the position of the VB edge was estimated to be E_V = -5.2 eV from the vacuum level. The FL-GeAs nanosheets exhibit the onset of E_{Ox} peak at 1 V, corresponding to E_V = -5.7 eV from the vacuum level. These values are consistent with the respective calculated values of E_V = -5.0 eV for N_L= 4 and E_V = -5.8 eV for N_L =1.

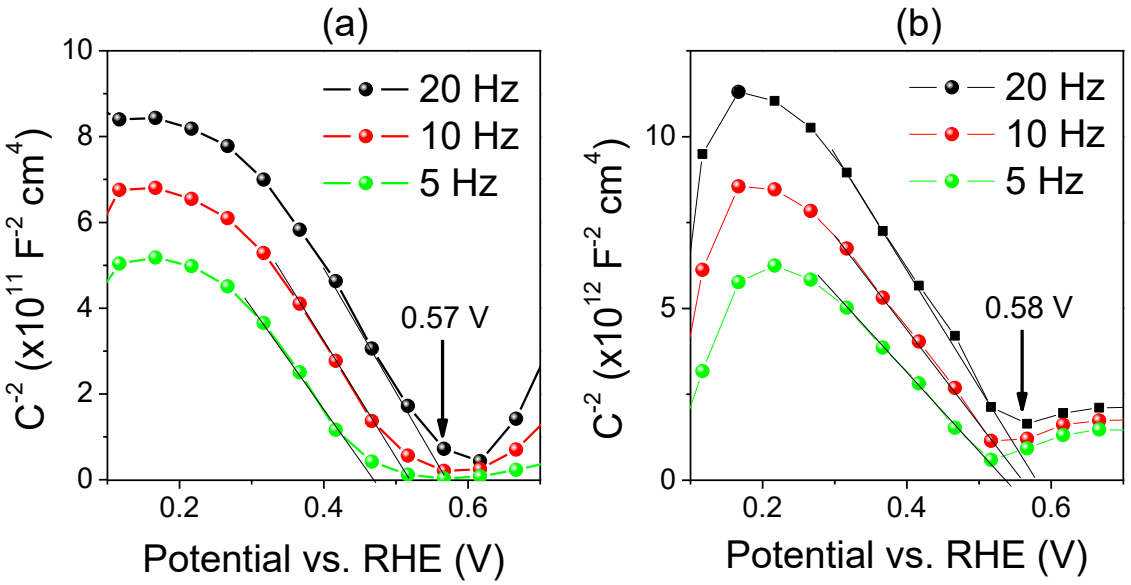

Figure S7. Mott–Schottky plots for the (a) ML-GeAs and (b) FL-GeAs nanosheets (on GC electrode) by impedance measurements in a 0.1 M Na_2SO_4/0.25 M NaOH electrolyte. The flat band potentials are obtained from the intercepts of the extrapolated lines.

The flat band potentials (E_{fb}) were investigated using Mott–Schottky (MS) plots, *i.e.*, the reciprocal of capacitance vs. the applied potential at 5, 10, and 20 Hz. These MS plots were measured by anodically sweeping the potential with an AC amplitude of 10 mV. For both materials, the linear plots with negative slope confirm the *p*-type character. The lines show the linear regions of the MS plots, and the E_{fb} values are obtained from the intercepts of the extrapolated lines. The E_{fb} values of ML- and FL-GeAs were determined to be nearly the same to each other (0.57 and 0.58 V vs. RHE at 20 Hz, respectively). On the basis of the ratio of the inverse slopes of the plots, the hole carrier density in FL-GeAs should be approximately ten times lower than in ML-GeAs.

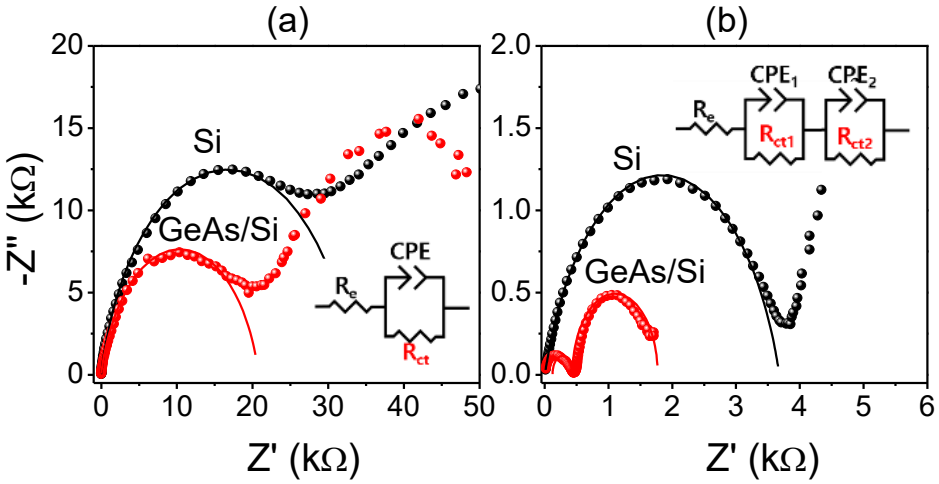

Figure S8. Nyquist plots of *n*-Si and *n*-Si/*p*-GeAs for EIS experiments in the range from 1 MHz to 0.1 Hz at 0 V (vs. RHE) under (a) dark and (b) the irradiation of AM1.5G 100 mW cm^{-2} using Xe lamp. The equivalent circuit is shown in the inset and the fitting curves are resprensent by the solid lines. The equivalent circuit is shown in the insets and the fitting curves are resprensent by the solid lines.

Electrochemical impedance spectroscopy (EIS) measurements in a 0.1 M Na_2SO_4/0.25 M NaOH electrolyte were carried out for the electrode by applying an AC voltage of 20 mV at a bias voltage of 1.23 V (vs. RHE). The *x*- and *y*-axes are the real part (Z′) and negative imaginary part (–Z′′) of the impedance, respectively. In dark, a semicircle in the Nyquist plot at high frequencies represents the charge transfer process, with the diameter of the semicircle reflecting the charge-transfer resistance. The simulation of EIS spectra (fitted lines) using an equivalent circuit model (inset) yielded the R_{ct} values. The fitting parameter R_e represents the internal resistance of the electrolyte, and CPE represents the constant-phase element related to the double-layer capacitance. The charge-transfer resistance (R_{ct}) between the electrode and electrolyte is 33.4 and 20.7 kΩ, respectively, for *n*-Si and *n*-Si/*p*-GeAs. The R_e value is about 400 Ω. Under light irradiation, two semicircles appear at high frequency range for *n*-Si/*p*-GeAs. For *n*-Si, the second circle also exists above the range of the plot. The simulation of EIS spectra (fitted line) using an equivalent circuit model (inset) yielded the two R_{ct} values (R_{ct1} and R_{ct2}), with corresponding CPE (CPE_1 and CPE_2). The sum of R_{ct1} and R_{ct2} is 2.3 kΩ. The *n*-Si shows R_{ct} = 89.5 kΩ in this range. The large R_{ct} value of Si NWs confirmed the sluggish charge transfer kinetics on the surface of Si. The smaller R_{ct} value of *n*-Si/*p*-GeAs indicates the much efficient charge transfer of photoelectrode and electrolyte interface.

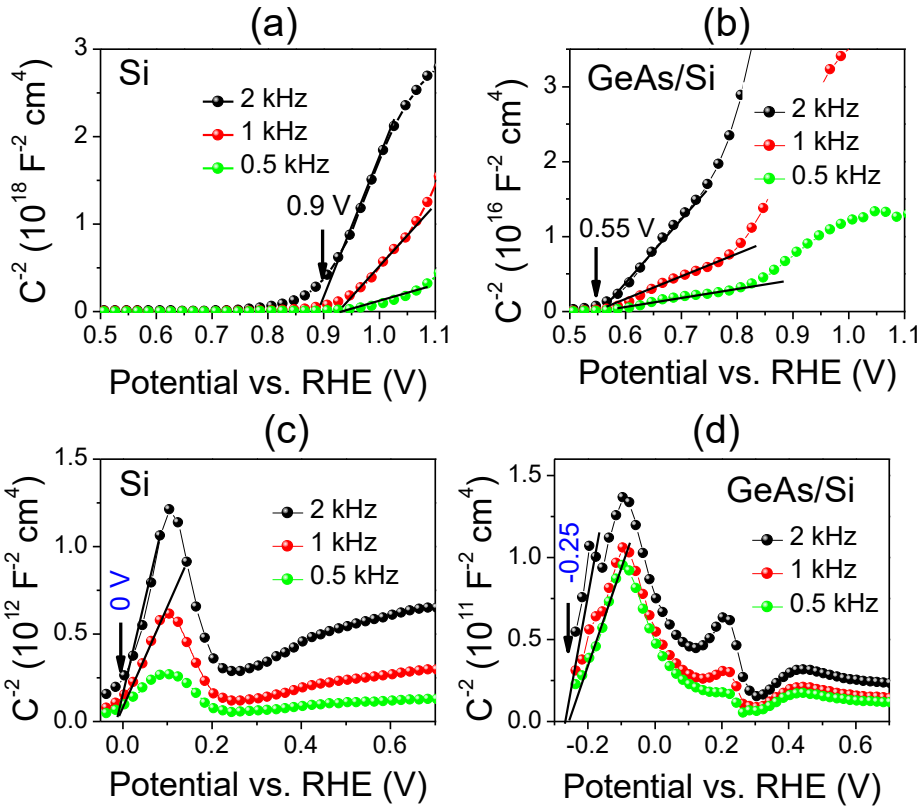

Figure S9. Mott-Schottky plots at 0.5, 1, and 2 kHz for (a) *n*-Si and (b) *p*-GeAs/*n*-Si in the dark, and (c) *n*-Si and (b) *p*-GeAs/*n*-Si under the irradiation of AM1.5G 100 mW cm^{-2} using Xe lamp. The flat band potentials are obtained from the intercepts of the extrapolated lines.

The flat band potentials (E_{fb}) in a 0.1 M Na_2SO_4/0.25 M NaOH electrolyte were investigated using Mott–Schottky (MS) plots. Under dark, the E_{fb} values of *n*-Si and *p*-GeAs/*n*-Si were determined as 0.9 and 0.55 V (vs. RHE), respectively. Under light irradiation, the E_{fb} values of *n*-Si and *p*-GeAs/*n*-Si were determined as 0 and -0.25 V (vs. RHE), respectively. This result means that the E_{fb} position is negatively shifted by about 0.3 V relative to that of *n*-Si. This shift is consistent with the cathodic shift of the onset potentials in the PEC cell. Therefore, the cathodic shift of the onset potential upon the FL-GeAs deposition is attributed to that of the E_{fb} position. The discrepancy between the E_{fb} and the photocurrent onset is likely due to the overpotential losses and voltage drop in the circuit.

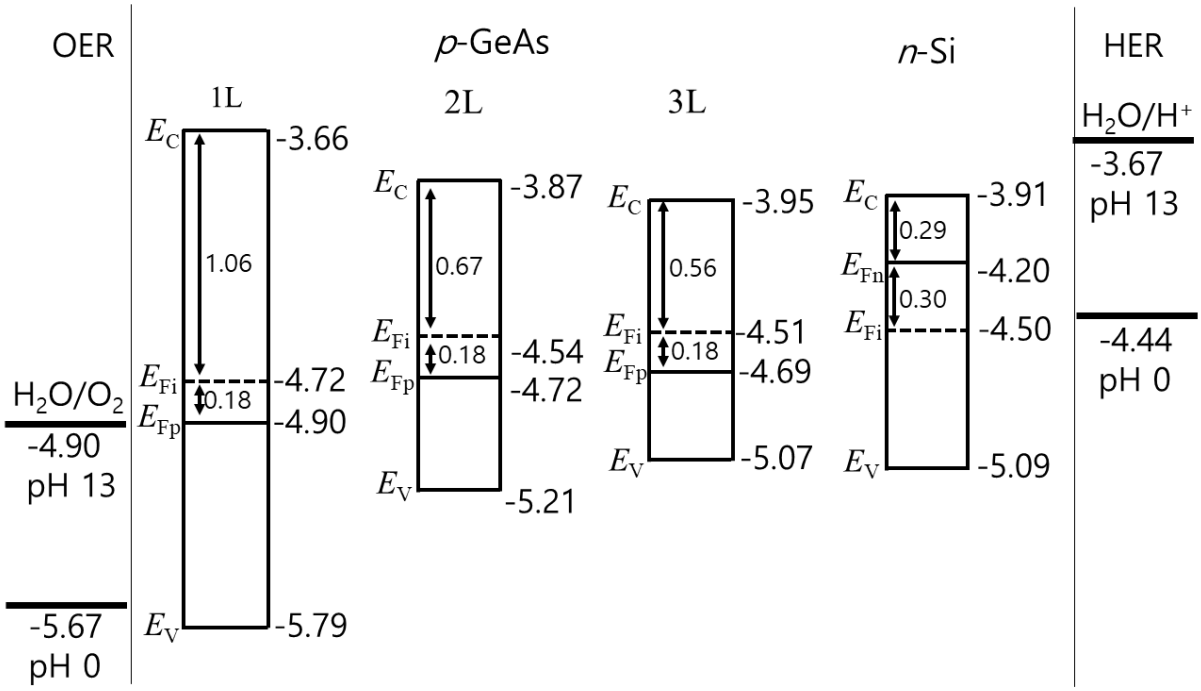

Figure S10. Band diagrams of the *p*-GeAs (1L-3L) and *n*-Si in vacuum before contact, and both diagrams are based on our calculation. The positions of CBM (E_V), VBM (E_C), and Fermi level (E_{Fi}, E_{Fp}, and E_{Fn}) versus the vacuum level are shown with the potentials of HER and OER at pH 0 and 13 (left and right ends).

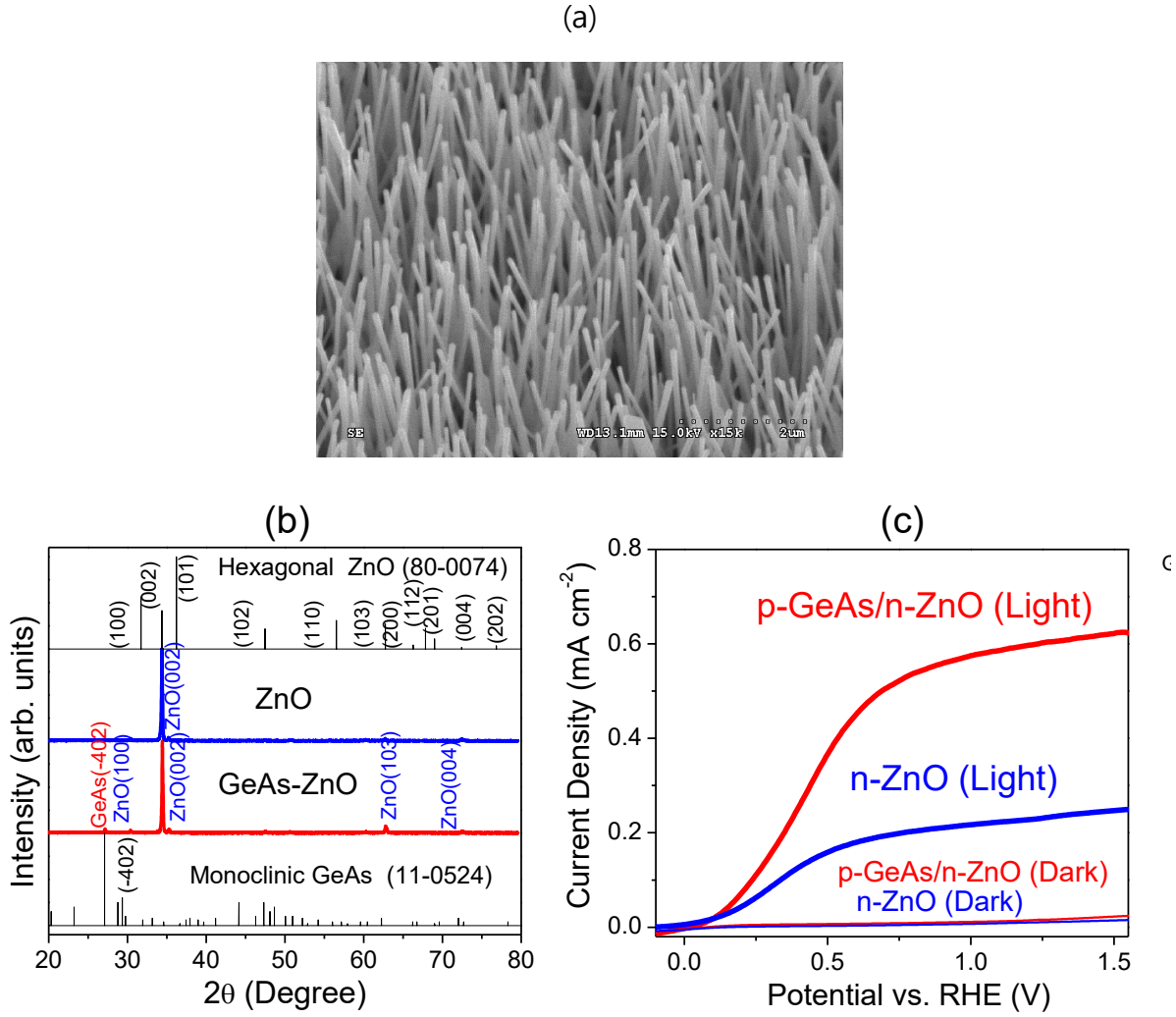

Figure S11. (a) SEM image of vertically aligned ZnO nanowire array (deposited FL-GeAs) on the ITO substrates. (b) XRD patterns of ZnO and GeAs/ZnO NW array. The displayed reference peaks are for ZnO (JCPDS No. 80-0074, a = 3.253 Å and c = 5.215 Å), and monoclinic phase GeAs (JCPDS No. 11-0524, $C2/m$, a = 15.59 Å, b = 3.792 Å, c = 9.49 Å, β = 101.28°). (c) Current density vs. potential (vs. RHE) for ZnO NW and *p*-GeAs/*n*-ZnO NW array photoanodes measured in a 0.1 M Na_2SO_4 (pH 6.2) electrolyte under AM1.5G (100 mW cm^{-2}) condition. Scan rate is 20 mV s^{-1}.

Vertically ZnO NW array was grown on ITO substrates using chemical vapor deposition of Zn powders under oxygen flow at 500 °C. The length of ZnO NW is 10 μm, and the diameter is 100 nm. The FL-GeAs nanosheets were deposited using the same method as that used for Si NWs. The GaAs/ZnO show the strongest (-402) peak of GeAs in the XRD pattern, confirming

that the deposition of FL-GeAs was successful. With the FL-GeAs deposition, the photocurrent density at 1.23 V was increased from 0.23 to 0.6 mA cm^{-2}.

References

S1. C. Barreteau, B. Michon, C. Besnard and E. Giannini, High-Pressure Melt Growth and Transport Properties of SiP, SiAs, GeP, and GeAs 2D Layered Semiconductors. *J. Crystal Growth*, 2016, **443**, 75-80.

S2. S. Yang, Y. Yang, M. Wu, C. Hu, W. Shen, Y. Gong, L. Huang, C. Jiang, Y. Zhang and P. M. Ajayan, *Adv. Funct. Mater.*, **2018**, 1707379.

S3. R. R. Gagné, C. A. Koval and G. C. Lisensky, Ferrocene as an Internal Standard for Electrochemical Measurements. *Inorg. Chem.*, 1980**, 19**, 2854-2855.